Novel Design and Implementation of a Neuromuscular Controller on a Hip Exoskeleton for Partial Gait Assistance

Sara Messara[1,2], Ali Reza Manzoori[1], Andrea Di Russo[1], Auke Ijspeert[1], and Mohamed Bouri[1]

***Abstract*— Exoskeletons intended for partial assistance of walking should be able to follow the gait pattern of their users, via online adaptive control strategies rather than imposing predefined kinetic or kinematic profiles. NeuroMuscular Controllers (NMCs) are adaptive strategies inspired by the neuromuscular modeling methods that seek to mimic and replicate the behavior of the human nervous system and skeletal muscles during gait. This study presents a novel design of a NMC, applied for the first time to partial assistance hip exoskeletons. Rather than the two-phase (stance/swing) division used in previous designs for the modulation of reflexes, a 5-state finite state machines is designed for gait phase synchronisation. The common virtual muscle model is also modified by assuming a stiff tendon, allowing for a more analytical computation approach for the muscle state resolution. As a first validation, the performance of the controller was tested with 9 healthy subjects walking at different speeds and slopes on a treadmill. The generated torque profiles show similarity to biological torques and optimal assistance profiles in the literature. Power output profiles of the exoskeleton indicate good synchronization with the users' intended movements, reflected in predominantly positive work by the assistance. The results also highlight the adaptability of the controller to different users and walking conditions, without the need for extensive parameter tuning.**

I. Introduction

Neuromuscular Controllers (NMCs) are powerful tools to reproduce physiological motor behaviors in simulations [1] and guide torque generation in assistive devices [2]. In an influential study, Geyer and Herr demonstrated that the kinematics and muscle activation observed in human locomotion could be reproduced without central commands using a controller relying purely on sensory feedback [3]. A similar controller with partial modifications was then proposed by Ong et al. [4], further highlighting the capability of reflex-based controllers in generating functional gaits. In these studies, the activation of sensory responses in the gait cycle is regulated by a state-machine mechanism enabling the activation of reflexes only in specific gait cycle phases. Different motor behaviors, like the modulation of gait speed, can also be achieved by modulating selected sensory reflex gains [5]. The idea of task- and phase-dependent regulation of the reflexes is supported by experimental observations in which different reflex responses in various motor tasks or gait phases were registered [6], [7].

The ability of NMCs to generate human-like gaits under different conditions in simulation, without requiring extensive sensory information, indicates them as good candidates for wearable robotic devices. This may also improve user acceptance and thus facilitate the adoption of the assistive devices for real-world use. Their ability to function with less sensory input allows for a simpler hardware structure and increased robustness to noise and failure.

In one of the first device implementations, a neuromuscular model was used to control a powered ankle-foot prosthesis in the stance phase, which allowed a person with transtibial amputation to walk on flat and inclined terrains [8]. The controller showed an inherent adaptivity to the terrain without explicit terrain detection or re-tuning. Following the promising results in simulation and prosthesis implementations, the first exoskeleton implementation of a NMC was reported in [9] for the ankle. Similar to the model proposed by Geyer and Herr [3], a finite-state machine (FSM) with two states (stance/swing) was used to modulate the reflexes. A percentage of the torque generated by the NMC was commanded to the exoskeleton assisting healthy people. The results showed reductions in the energetic cost of walking and muscle activities, while largely preserving the natural gait patterns.

Several similar implementations have been reported later for assisting subjects with spinal cord injury on different devices, including a hip-knee gait trainer [10], an ankle exoskeleton [11], and a full-leg exoskeleton [12]. The results indicated the ability of the NMC to assist users with a range of impairments to walk at various speeds, without imposing a pre-defined movement [2]. However, these implementations used a two-state FSM, which cannot capture the potential modulations of the reflex pathways in sub-phases within stance and swing, such as those proposed by Ong et al. [4]. Furthermore, all of the aforementioned variants of the NMC used the Hill-type model for the virtual muscles, which is a three- or four-element model of the biological muscles. While the elaborateness of this model is necessary for reproducing the dynamic behavior of the biological muscles, its utility for assistive controllers is unclear. The added complexity by this model, which can also lead to numerical issues in real-time implementations, might not be justified [13].

In this work, we present a novel design of the NMC based on a 5-state FSM and a simplified version of the virtual muscle model. In terms of functionality, the fine-

*AM received funding from the European Union's Horizon 2020 research and innovation programme under the Marie Sklodowska-Curie Grant Agreement No. 754354.

[1]All of the authors are with the Biorobotics Laboratory (BioRob) of EPFL, 1015 Lausanne, Switzerland. {ali.manzoori, andrea.dirusso, auke.ijspeert, mohamed.bouri}@epfl.ch

[2]SM is also with UPSSITECH School of Engineering at the Université Toulouse III Paul Sabatier, France. sara.messara.private@gmail.com

grained FSM provides more freedom in adjusting the emergent assistive torque profiles, while the simplifications of the virtual muscle model allow for a more straightforward implementation. The controller was implemented on a hip exoskeleton and tested with healthy subjects in treadmill-walking experiments at various speeds and slopes. The main goal was to firstly validate the performance of the novel NMC with different users, and then to study its adaptability across different speeds and slopes.

II. Methods

A. Novel Neuromuscular Controller

1) Virtual muscles: The Hill-type model is chosen as a basis, to which we contribute by proposing simplifications and a new computational approach. Descriptions of the base model and the usual computational approach used in the literature can be found in [3] and [14]. In this article, the same notations are kept, therefore only contributions to equations will be presented.

In our implementation, the serial element which models the series elasticity of the tendon, is assumed to have a constant length. This is justified by the high biological stiffness of the tendon, estimated to be around $150\,\mathrm{kN}\cdot\mathrm{m}^{-1}$ on average [15], indicating that the tendon length will not deviate significantly from the slack length, l_{slack} in normal walking. With this simplification, the serial element length, l_{se}, and its rate of change, v_{se}, become constants, reducing the system's degrees of freedom by half. This allows to compute the Contractile Element (CE) length, l_{ce}, and its rate of change, v_{ce}, from the kinematic equation of the muscle length and its analytical derivative:

$$\begin{aligned} l_{ce} &= l_{mtu} - l_{se} \\ &= l_{opt} + l_{slack} + \Delta l_{mtu}(\theta) - l_{se} \end{aligned} \tag{1}$$

$$v_{ce} = \frac{d\Delta l_{mtu}(\theta)}{d\theta} . \frac{d\theta(t)}{dt} \tag{2}$$

where l_{mtu}, l_{opt} and θ denote the total muscle-tendon unit length, the optimum CE length, and the joint angle, respectively. The value of $\Delta l_{mtu}(\theta)$ for the hip joint muscles is derived as in [3] based on the muscle's moment arm r_0 and reference angle θ_{ref}, and replaced in Eqs. (1) and (2):

$$l_{ce} = l_{opt} + l_{slack} + r_0.(\theta - \theta_{ref}) - l_{se} \tag{3}$$

$$v_{ce} = r_0.\dot{\theta} \tag{4}$$

From the resolution of the CE state, it is possible to calculate the force generated by the CE (F_{ce}) using the force-length and force-velocity relationships given in [14]. The force generated by the hip muscle is ultimately:

$$F_{mtu} = F_{pe} + F_{ce} - F_{be} \approx F_{ce} \tag{5}$$

The last approximation in Eq. (5) is based on the length equality between the buffer element (l_{be}) and the parallel element (l_{pe}), resulting in the cancellation of the forces generated by the two passive elements. The muscle's torque around the hip is thus given by:

$$\tau_{mtu} = F_{mtu}.r_0 \tag{6}$$

This method, that we call the derivative approach, contrasts with the integral computational approach used in the base model. It prevents several approximations, such as the iterative computation of the l_{se}, the estimation of the l_{ce} from numerically integrating v_{ce}, and the computation of v_{ce} from the inversion of the force-velocity relationship. The latter is not recommended in real-time embedded hardware implementations, given the limited precision. This ultimately yields a more accurate muscle state estimation and a more computationally efficient scheme.

The virtual muscles used in this work are also different from the conventional NMC implementations that included a hip joint with 3 hip muscle groups [10]. We only kept the mono-articular muscles, since the controller is targeting a hip-only exoskeleton without sensing at the knee level. This restricted the choice to the iliopsoas (ILPS) as a hip flexor and gluteus maximus (GLU) as a hip extensor muscle. The baseline assistance torque is the resultant torque of the contributions of both muscles, multiplied by a gain $G_{s,v}$:

$$\tau_{assist} = G_{s,v}.(\tau_{GLU} + \tau_{ILPS}) \tag{7}$$

$G_{s,v}$ is tuned depending on the ground slope (s) and walking velocity (v), since the original NMC was designed to assist walking on flat ground at a medium speed. The torque was further scaled by the body mass of each subject.

2) Reflexes: Reflexes were modulated as a function of the gait phase, using one 5-state FSM per leg, which allows to encapsulate the dynamic nature of the human reflexes over the gait cycle. The considered states are: Early stance (ES), mid-stance (MS), pre-swing (PS), initial swing (IS) and landing preparation (LP). The ES, MS, PS and IS states for each leg were triggered by detecting the ipsilateral heel-strike, the contralateral toe-off (indicating the start of single support), the contralateral heel-strike (marking the start of double support), and the ipsilateral toe-off, respectively. The detection was based on based on a threshold of $10\,\mathrm{N}$ on the foot load signal from insole Force-Sensitive Resistors (FSRs). The LP was triggered by the the flexion/extension angular velocity falling below $-1\,\mathrm{deg/s}$, which indicates the change of direction of the leg prior to landing.

A novelty of our implementation is to rely on length feedback and constant inhibition instead of the commonly implemented force feedback reflex [14]. The choice of the length feedback is motivated, first, by the smoothness of the length signal compared to the velocity of the CE. Second, in Ong et al.'s work [4], a set of velocity and length reflexes were shown to be sufficient for a broad range of gait speeds in simulation. The selected reflexes for each phase are presented in Table I. Depending on the phase, the applied stimulation is given by a variant of the following equation (the terms in brackets are phase-dependent):

$$Stim(t) = Stim_0\ [+G_l.l_{ce}(t - \delta t)]\ [-C] \tag{8}$$

where $Stim_0$ is the "basal" activation of the muscle, G_l is the length reflex gain, $\delta t = 5\,\mathrm{ms}$ is a constant simulating the neural signal delays, and C is a constant inhibition term.

TABLE I

SELECTED REFLEXES AS A FUNCTION OF STATE. L^+ REFERS TO THE POSITIVE LENGTH FEEDBACK, AND C^- TO THE CONSTANT INHIBITION

	ES	MS	PS	S	LP
Glu.	L^+	L^+, C^-	L^+, C^-	L^+, C^-	L^+
Ilps.	$basal$	L^+	L^+	L^+	L^+, C^-

3) Parameter Tuning: The model includes 18 muscle characteristic parameters and 13 reflex gains per muscle, adding up to 62 parameters in total by assuming symmetry between the legs. For the muscle characteristics, we based the tuning on two former studies [3], [4]. Data-driven simulations in MATLAB and Simulink (Mathworks Inc., USA) were used to test the muscles using angular position and velocity data recorded previously. Then, from the analysis of the various state variables (l_{CE}, v_{CE}, torques, stimulations, and activations), we recursively isolated a set of parameters to be re-tuned.

For the reflex gains, it was not possible to rely on previous studies firstly because we proposed a new combination of reflexes that had not been tested in any previous simulation or experiment. Furthermore, the gains influence greatly the magnitude of the generated torque commands, and therefore the torque limits of the target exoskeleton must be taken into account. The method used to tune these parameters was therefore in-vivo hardware and system in the loop simulations with hand tuning. The tuning criteria of the inhibition constants and gains were, first, the continuity and smoothness of curves despite discrete state transitions and second, the mimicry of the biological torque profiles (from [16]) in terms of curve tendency, characteristic times, magnitude ratio and muscle activations.

Lastly, the tuning of $G_{s,v}$ was inspired by the biological magnitude adaptation of the hip torque [16], [17]. It was set to 0.8 , 1 and 1.15 respectively for the slow, normal and fast speed conditions on level surface, and 1.15 for incline. The tuning was performed prior to the experiments, and the same parameters were used for all subjects.

B. Experimental Setup and Protocol

A bilateral hip exoskeleton prototype (e-Walk V1, Fig. 1) was used to test the controller with human subjects. The device is actuated with BLDC motors providing nominal and peak torques of 13 and $35\,\mathrm{N \cdot m}$ respectively. An efficient 6:1 planetary reducer allows for easy back-driving of the motors by the wearer (back-driving torques of less than $0.6\,\mathrm{N \cdot m}$ RMS for movements up to $2\,\mathrm{Hz}$). The motors are connected to thigh cuffs with thin carbon-fiber-reinforced beams that are only stiff around the flex/extension axis. Due to the flexibility of the beams outside of the sagittal plane, abd/adduction and int/external rotations remain possible.

The exoskeleton is controlled by an embedded computer (BeagleBone Black, BeagleBoard.org Foundation, USA) running real-time Linux. The setup includes a range of sensors, namely absolute joint angle encoders, insole FSRs, and actuator current sensors, all of which are read and logged

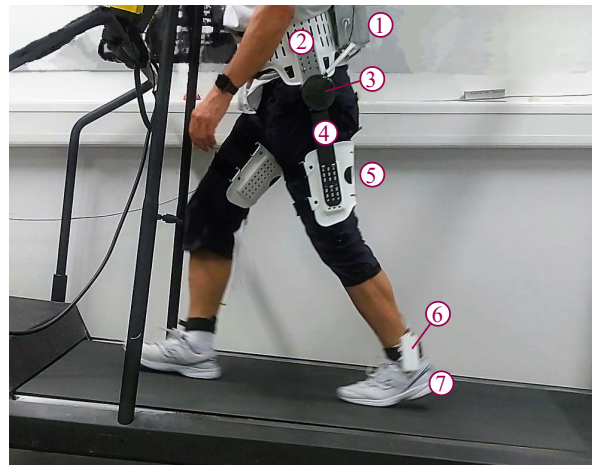

Fig. 1. The experimental setup, showing a subject walking on the inclined treadmill while wearing the exoskeleton. The hip exoskeleton consists of: (1) back box including embedded electronics and batteries, (2) waist interface, (3) hip joint actuator, (4) thigh segment, (5) thigh cuff, (6) insole FSR amplifier, and (7) shoes with insole FSRs.

by the embedded computer. Thanks to the high efficiency of the transmission, the actuator currents were used to estimate the applied torques using conversion coefficients found in benchtop tests with torque sensors. Thus, the commanded torques were converted to currents commanded to the motors, enforced with a current control loop at $32\,\mathrm{kHz}$. The main control loop was set to run at $500\,\mathrm{Hz}$, which is sufficient given the dynamics of human gait.

The goal of the experiment was firstly to validate the novel NMC in terms of the emerging assistive torque profiles and their effect on the user's kinematics, as well as the adaptability of the torques to various walking conditions. The protocol was approved by the EPFL Human Research Ethics Committee. Nine able-bodied adults (5 females, 4 males, age: 27 ± 2.3 years, weight: $65.0 \pm 8.4\,\mathrm{kg}$) took part in the experiments. All subjects provided written informed consent prior to the experiment. The participants who had no previous experience with the exoskeleton ($n = 5$) were asked to walk for $2\,\mathrm{min}$ on a treadmill (N-Mill, Forcelink B.V., Netherlands) at different speeds while wearing the exoskeleton prior to the main experiment.

The protocol included 8 conditions at varying speeds and inclines, 4 with the exoskeleton in active mode (conditions "C<i>") and 4 in transparent mode (conditions "C<i>t"). The transparent conditions, in which the motors of the exoskeleton were driven in zero-torque mode, were used as the baseline of each subject's kinematics. The first three pairs of conditions assessed the adaptability of the controller to walking on a level surface at various speeds: slow at $0.8\,\mathrm{m \cdot s^{-1}}$ (C1, $2.5\,\mathrm{min}$ and C1t, $1.5\,\mathrm{min}$), normal at $1.25\,\mathrm{m \cdot s^{-1}}$ (C2, $2.5\,\mathrm{min}$ and C2t, $1.5\,\mathrm{min}$), and fast at $1.8\,\mathrm{m \cdot s^{-1}}$ (C3, $2\,\mathrm{min}$ and C3t, $1.5\,\mathrm{min}$). The 4th pair of conditions tested the adaptability to inclines and consisted in walking at $1.25\,\mathrm{m \cdot s^{-1}}$ on a 10% upward slope (C4, $2\,\mathrm{min}$ and C4t, $1\,\mathrm{min}$). The subjects were given sufficient time to rest between the conditions.

C. Data analysis

Data for each subject were segmented into single gait cycles, based on heel-strikes detected from the insole pressure sensor signals. The segmentation was performed separately for each leg using the ipsilateral heel-strikes. The assistive powers were calculated from the estimated motor torques and the angular velocities estimated from the encoders. The works per stride were then obtained by numerically integrating the powers. After verifying the normal distribution of the results using one-sided Kolmogorov-Smirnov test, statistical significance of the differences in the produced work between conditions was first tested using a repeated measures one-way ANOVA at 5% significance. In case of a significant outcome, Wilcoxon's matched pairs signed rank test was used for pair-wise post-hoc comparisons at 5% significance. All data analysis was performed in MATLAB. The convention of signs for torque and angles is positive in the flexion direction and negative in extension.

III. Results

The average profiles of hip angle for each assisted condition compared to the transparent are shown in Figs. 2A–D. In all of the assisted conditions, a tendency toward higher extension angles is observed in the angle profiles compared to transparent, also resulting in an increase of about $5\,\mathrm{deg}$ on average in the overall range of motion. The assisted conditions display a markedly higher retraction in the angles prior to heel-strike, particularly in C1–C3, highlighted in Fig. 2.A to 2.D.

The average torques generated by the NMC are presented in Fig. 2.F. The profiles show a period of extension from LP to MS, followed by a period of flexion from PS to LP. The magnitude of torques in the extension direction are higher.

The angle and torque profiles showed notable variations, particularly between the subjects. The median inter-subjects kinematics standard deviations across all conditions were: $4.2\,\mathrm{deg}$ for the hip angle, $40.44\,\mathrm{deg/s}$ for the hip velocity and $14\,\mathrm{mN}\cdot\mathrm{m}\cdot\mathrm{kg}^{-1}$ for the normalised torque.

The average exoskeleton output power profiles and work per stride values are presented in Figs. 3.A and 3.B, respectively. The power values are almost constantly positive, as also reflected in the negligible magnitude of negative works. The power delivery is mostly happening in ES, IS, and LP. The work values show an increasing trend with speed and slope, with the highest amount of work performed in C4.

The activation signals of the virtual muscles are shown in Fig. 3.C, with the typical activation timings of the biological equivalents marked for comparison. The extensor (GLU) is mostly active during LP to MS, with an activation peak in ES, whereas the flexor (ILPS) is mostly active from MS to IS. Furthermore, the magnitude of the extensor activation is around 30% higher than the flexor, in line with the trends observed in the torques.

IV. Discussion

The performance of the NMC was tested over an extensive range of walking patterns, to which it adapted by computing the assistive torques online without the need for specific tuning (apart from the linear scaling gain, $G_{s,v}$) or predefined torque profiles. The trends of the hip kinematics did not show major deviations from non-assisted walking, except for some jitter observed in the hip angle during ES and MS. The tendencies toward extension in the assisted conditions agree with the common pattern in partial assistance studies such as [19], since the magnitude of extension torques are generally higher than flexion.

The jittering in the angle profiles was due to the movement of the exoskeleton attachments with respect to the body, as evidenced by the concurrence of the jitter with the reduction of the extension torque on the ipsilateral and the period of peak flexion torque on the contralateral leg. Since an off-the-shelf corset intended for passive orthoses was used as the waist attachment, rapid changes of the torques caused visible deformations in the interface leading to movement of the motors relative to the body.

The exoskeleton power, and consequently the delivered work, were predominantly positive across all conditions, with negligible amounts of negative work. The positive work was on average 30 times higher than the negative work. Since the magnitudes of the applied torques were not high enough to enforce a movement on the user, the positive powers and works are good indicators that the assistive torques were synchronized with the intended movements of the users. Furthermore, the total work and the peaks of powers grew with the speed and incline, demonstrating that the assistance adapted to the level of effort in the various conditions. The highest negative work occurred in the C3 condition with a value of $-2.4\,\mathrm{mJ}\cdot\mathrm{kg}^{-1}$ against $72.8\,\mathrm{mJ}\cdot\mathrm{kg}^{-1}$ of positive work. The short period of negative power in C3 is due to the jitter induced by the relative movement of the exoskeleton interface during ES, and therefore has little effect on the user. This condition also had the highest kinematic jitter due to the high walking speed, which validates the former hypothesis.

We evaluated the generated torques by comparing them to torque profiles from the literature. One basis for comparison was the assistance torque profiles obtained from human-in-the loop (HitL) optimization for metabolic cost reduction on a range of slopes [19].Comparisons against the trends observed in biological torques were also made. The considered features were the overall profile trends, characteristic times (in percentage of the gait cycle), and magnitudes. The general trend of the torque and phase transitions of the assistance matched their biological counterparts [16]–[18]. The beginning of the ES corresponded to 0%, the the MS started on average at 10.64%, the TS at 49.57%, the IS at 60.78% and the terminal stance (TS) or LP at 89.24%. These results are consistent with the reported biological data as in [18] which validates the controller's FSM phase synchronization. The inter-subject variance of the characteristic times did not exceed 2%. The peak of extension for the flat conditions at various speeds happened on average at 8% which falls within the biological range of $6\pm4\%$ [16] and remains fairly close to the range reported in [19], i.e., between 9.1 to 11.5%. For the inclined condition, the peak timing coincided with the

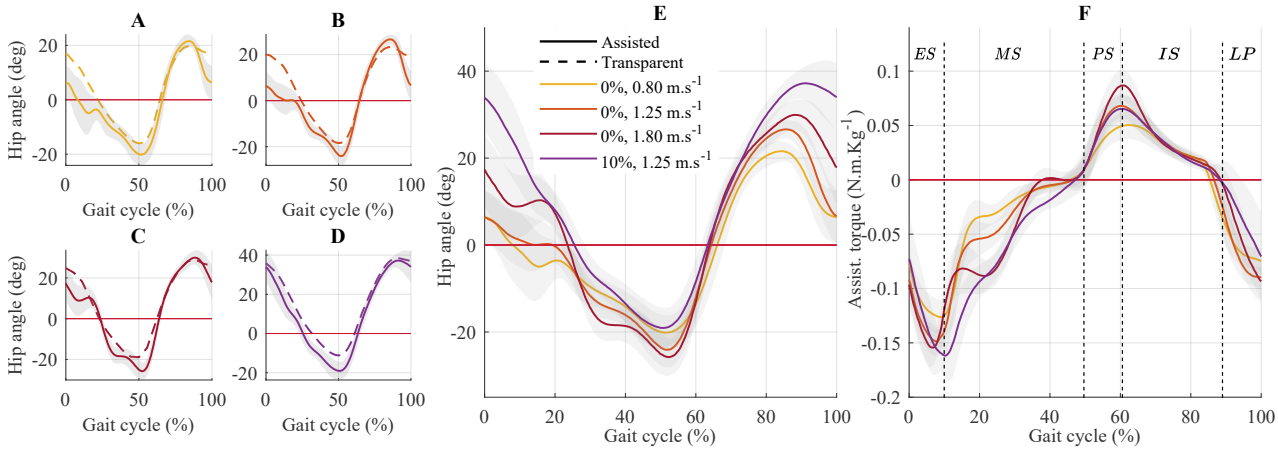

Fig. 2. (A)-(D) Averaged hip angles profiles across all subjects ($n = 9$) for the eight conditions, the dashed lines represent the unassisted conditions C<i>t and the continuous lines the assisted conditions C<i>. (E) Average hip angle profiles across subjects in the four assisted conditions. (F) Average assistance torque for the four assisted conditions, also showing the states of the FSM.

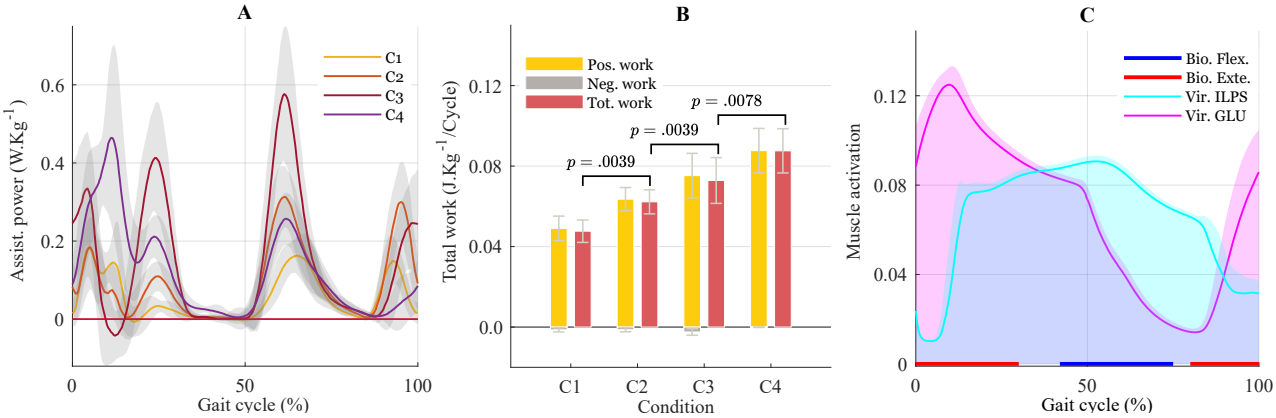

Fig. 3. (A) Average power for the four assisted conditions C<i>, the shaded areas represent the standard deviations. (B) Average positive, negative and total work per cycle for each assisted condition C<i>, along with the p-values for the pair-wise differences from Wilcoxon's matched pairs signed rank test. (C) The virtual muscle activations, with the active ranges of the biological hip flexors and extensors from [18] marked on the horizontal axis.

average value of 10% obtained from HitL optimisation.

The extension to flexion zero crossing of the torques happened on average at 47% which is in the limits of the biological torque profile [16]. The extension torques decreased to a near-zero ($< 0.01\,\mathrm{N{\cdot}m{\cdot}kg^{-1}}$) value starting around 35%, similar to the trends observed in the HitL-optimised torques. This characteristic time tended to increase with both the walking speed and ground slope, in line with the biological behavior reported in [17]. Moreover, this suggests a longer duration of extension assistance when the user increases the hip extension range and duration. The peak of flexion happened on average at 61%, which is in between the timing of the average biological torques (52%) [16] and the HitL-optimised profiles (66%) [19]. The flexion to extension zero crossing happened on average at 87% which is close to the HitL value of 88% [19]. This characteristic time also tended to increase with both the speed and slope, in agreement with biological trends [17]. This suggests that the controller adapts to the variation in the ranges of motion by providing longer flexion assistance when the subject increases the hip flexion range and duration.

In terms of magnitudes, the average extension to flexion ratio was 2.45 (minimum: 1.87, maximum: 3). In the biological torques, this ratio is above 1.5 [16], since extension torques contribute to weight bearing, thus requiring more effort. In the HitL torques, the average ratio was 2.3, with a minimum value of 1.6 and a maximum of 3 [19]. The extension peak increased with both the speed and slope. The flexion peak increased with the speed and decreased with the slope (compared to the flat ground at the same speed). Both behaviors have been observed biologically [17], which confirms the magnitude adaptability of the controller. Note that before applying $G_{s,v}$, the NMC showed a good adaptability in terms of characteristic times, but the magnitude adaptation was not sufficient. This shortcoming was improved by introducing this adaptation gain, which was tuned manually in this study.

The activation peak timing of the GLU matched its biological counterpart [16], [18]. The burst of activity for this virtual muscle begins during LP, reaches its peak during ES

and continues until the middle of MS, which corresponds well to the period when the hip joint contributes to the forward acceleration of the body. The peak of the ILPS activation coincides with the biological range of hip flexors activation. It was active during the biological activation range (PS and IS) and had a larger activation band extending to the MS and the end of the IS. This same result was previously reported in some gait simulation studies as in [4]. One important property is that, the 2 virtual muscles exhibit an antagonist behavior having inverted activation and deactivation tendency which aligns with their biological antagonism. A period of mild co-conctraction happens during the single-support period (10–50%), which would lead to a higher stiffness of the joint and thus higher stability of the body. In terms of activation magnitude, the virtual GLU had a higher activation then the ILPS, given the fact that the extension requires more effort because of the load bearing.

A main limitation of this study was the lack of direct torque measurement in the exoskeleton, reducing the accuracy of the applied torques and the analyses based on them. Also, the imperfect fitting of the prototype exoskeleton negatively affected the joint angle measurements and the transfer of torques to the user. Another limitation was the lack of biological measurements, such as metabolic rate or muscle activities to asses the contribution of the assistance to reducing user's effort. Lastly, the adaptivity of the NMC can be significantly improved by replacing the manually tuned gain $G_{s,v}$ with an adaptive gain.

V. Conclusion

This study presented a novel modular approach for the implementation of the NMC and its validation on a partial assistance hip exoskeleton. The main contributions were *(i)* the proposition of a new 5-state FSM for gait synchronisation, *(ii)* the simplification of the Hill muscle model, resulting in a new analytical state resolution method with improved computational efficiency, and *(iii)* introduction of a new set of length reflexes for the control of the chosen virtual muscles. The experimental results validated the adaptability of the controller to various walking speeds and ground levels, particularly in terms of assistance timing. Predominantly positive power profiles demonstrated a good synchronization with the users. The hip kinematics showed similar trends to normal walking, with considerable inter-subject variability indicating the controller's adaptation to each user's gait.

Acknowledgment

We would like to thank Dr Romain Baud and Dr Olivier Pajot for their contributions to the preparation of the software and hardware of the exoskeleton, and Olivier Clerc for his help in carrying out the experiments.

References

[1] A. Prochazka, S. Gosgnach, C. Capaday, and H. Geyer, "Neuromuscular models for locomotion," in *Bioinspired Legged Locomotion: Models, Concepts, Control and Applications*. Elsevier Inc., Nov. 2017, p. 401.

[2] N. L. Tagliamonte, A. R. Wu, I. Pisotta, F. Tamburella, M. Masciullo, M. Arquilla, E. H. F. van Asseldonk, H. van der Kooij, F. Dzeladini, A. J. Ijspeert, and M. Molinari, "Benefits and potential of a neuromuscular controller for exoskeleton-assisted walking," in *Wearable Robotics: Challenges and Trends*, ser. Biosystems & Biorobotics, J. C. Moreno, J. Masood, U. Schneider, C. Maufroy, and J. L. Pons, Eds. Cham: Springer International Publishing, 2022, pp. 281–285.

[3] H. Geyer and H. Herr, "A muscle-reflex model that encodes principles of legged mechanics produces human walking dynamics and muscle activities," *IEEE Transactions on Neural Systems and Rehabilitation Engineering*, vol. 18, no. 3, pp. 263–273, 2010.

[4] C. F. Ong, T. Geijtenbeek, J. L. Hicks, and S. L. Delp, "Predicting gait adaptations due to ankle plantarflexor muscle weakness and contracture using physics-based musculoskeletal simulations," *PLoS computational biology*, vol. 15, no. 10, p. e1006993, 2019.

[5] A. Di Russo, D. Stanev, S. Armand, and A. Ijspeert, "Sensory modulation of gait characteristics in human locomotion: A neuromusculoskeletal modeling study," *PLoS computational biology*, vol. 17, no. 5, p. e1008594, 2021.

[6] P. K. Mutha, "Reflex circuits and their modulation in motor control: a historical perspective and current view," *Journal of the Indian Institute of Science*, vol. 97, pp. 555–565, 2017.

[7] A. Prochazka, "Proprioceptive feedback and movement regulation," *Comprehensive Physiology*, pp. 89–127, 2010.

[8] M. F. Eilenberg, H. Geyer, and H. Herr, "Control of a powered ankle–foot prosthesis based on a neuromuscular model," *IEEE Transactions on Neural Systems and Rehabilitation Engineering*, vol. 18, no. 2, pp. 164–173, Apr. 2010.

[9] F. Dzeladini, A. R. Wu, D. Renjewski, A. Arami, E. Burdet, E. van Asseldonk, H. van der Kooij, and A. J. Ijspeert, "Effects of a neuromuscular controller on a powered ankle exoskeleton during human walking," in *2016 6th IEEE International Conference on Biomedical Robotics and Biomechatronics (BioRob)*, Jun. 2016, pp. 617–622.

[10] A. R. Wu, F. Dzeladini, T. J. H. Brug, F. Tamburella, N. L. Tagliamonte, E. H. F. van Asseldonk, H. van der Kooij, and A. J. Ijspeert, "An adaptive neuromuscular controller for assistive lower-limb exoskeletons: A preliminary study on subjects with spinal cord injury," *Frontiers in Neurorobotics*, vol. 11, 2017.

[11] F. Tamburella, N. L. Tagliamonte, I. Pisotta, M. Masciullo, M. Arquilla, E. H. F. van Asseldonk, H. van der Kooij, A. R. Wu, F. Dzeladini, A. J. Ijspeert, and M. Molinari, "Neuromuscular controller embedded in a powered ankle exoskeleton: Effects on gait, clinical features and subjective perspective of incomplete spinal cord injured subjects," *IEEE Transactions on Neural Systems and Rehabilitation Engineering*, vol. 28, no. 5, pp. 1157–1167, May 2020.

[12] C. Meijneke, G. van Oort, V. Sluiter, E. van Asseldonk, N. L. Tagliamonte, F. Tamburella, I. Pisotta, M. Masciullo, M. Arquilla, M. Molinari, A. R. Wu, F. Dzeladini, A. J. Ijspeert, and H. van der Kooij, "Symbitron exoskeleton: Design, control, and evaluation of a modular exoskeleton for incomplete and complete spinal cord injured individuals," *IEEE Transactions on Neural Systems and Rehabilitation Engineering*, vol. 29, pp. 330–339, 2021.

[13] N. Van der Noot, F. Dzeladini, R. Ronsse, and A. J. Ijspeert, "Simplification of the hill muscle model computation for real-time walking controllers with large time steps," in *Dynamic Walking*, Zürich, Switzerland, 2014.

[14] H. Geyer, A. Seyfarth, and R. Blickhan, "Positive force feedback in bouncing gaits?" *Proceedings of the Royal Society B: Biological Sciences*, vol. 270, no. 1529, pp. 2173–2183, Oct. 2003.

[15] C. N. Maganaris and J. P. Paul, "In vivo human tendon mechanical properties," 1999.

[16] D. A. Winter, *The Biomechanics and Motor Control of Human Gait: Normal, Elderly and Pathological*. Waterloo, Ont.: University of Waterloo Press, 1991.

[17] E. Reznick, K. R. Embry, R. Neuman, E. Bolívar-Nieto, N. P. Fey, and R. D. Gregg, "Lower-limb kinematics and kinetics during continuously varying human locomotion," *Scientific Data*, vol. 8, no. 1, p. 282, 2021.

[18] J. Perry, J. R. Davids *et al.*, "Gait analysis: normal and pathological function," *Journal of Pediatric Orthopaedics*, vol. 12, no. 6, p. 815, 1992.

[19] P. W. Franks, G. M. Bryan, R. Reyes, M. P. O'Donovan, K. N. Gregorczyk, and S. H. Collins, "The effects of incline level on optimized lower-limb exoskeleton assistance: A case series," *IEEE Transactions on Neural Systems and Rehabilitation Engineering*, vol. 30, pp. 2494–2505, 2022.